



**GEORGIA
SOUTHERN
UNIVERSITY**

2021 Cast in Steel Competition: Casting Thor's Hammer



Shelton Fowler, J. Chandler Liggett, Daniel Garcia

Faculty Advisor: Dr. Mingzhi Xu

Partner Foundry: Carolina Metal Casting



Table of Contents:

1. Introduction

1.1 Introduction to Thor's Hammer

1.2 Introduction to Design Requirements

1.3 Introduction to Bimetal Castings

2. Design and Development

2.1 Designing Thor's Hammer

2.2 Lightweight Structure Design

2.3 Alloy Selection and Bimetal Casting Design

2.4 Hammer Structural Design

2.5 Casting Process Selection and Design

2.6 Gating and Riser Design

2.7 Heat Treatment Design

3. Manufacturing Methods

3.1 Additive Manufacturing of Patterns

3.2 Investment Shell Production

3.3 Sand Mold Production

3.4 Casting Process

3.5 Postprocessing

3.6 Heat Treatment

3.7 Final Preparation

4. Results and Discussion

4.1 Final Alloy Composition

4.2 Microstructure Analysis and the Bimetal Interface

4.3 Analysis of Fusion Defects in the Hammer Casting

5. Conclusion

1. Introduction

1.1 Introduction to Thor's Hammer

Thor's hammer, arguably the most iconic relic from Nordic mythology, continues today to be well known as both a symbol of classic Nordic mythology and an icon from the popular Marvel comic superhero. Thus, what makes a hammer a true "Thor's Hammer" differs widely from individual to individual based on their personal backgrounds. To one person, Thor's Hammer may conjure images of the classic Nordic symbol for Mjolnir, the name of Thor's Hammer, while for others Thor's Hammer is always seen in the hand of Chris Hemsworth. Both depictions however have together carved a distinct legacy behind Thor's Hammer which have formed it into the icon which it is today.

According to Nordic mythology, Thor's Hammer was the weapon of the god of thunder, Thor. The most notable property of the hammer was, when thrown, the hammer would always return to the hand of Thor. [1] The hammer was Thor's chief weapon and was used to defend Asgard and to defeat the giants, or *jötunn*. [1] First and foremost, the hammer was a weapon of war, but it was also an instrument of blessing according to Nordic culture. Several historical sources indicate that the hammer was used to consecrate and to bless in formal ceremonies marking events such as marriage, birth, and death. [1] What is unique mythologically about the hammer is that it was used as both an instrument of death and of consecration. One famed historian refers to the Nordic idea of the separation between the sacred and the profane. [1] [2] Thor's hammer was used often to delineate the two, banishing the profane and consecrating the sacred. Thus, according to Nordic mythology Thor's Hammer was functionally a weapon, but symbolically was so much more. It was both a weapon of war and an instrument of sacred rites.

The hammer is depicted symbolically as shown in Figure 1. A sketch of an actual historical Thor's Hammer amulet is shown here, recovered from an archaeological site in Sweden. Traditional Thor's hammer depictions show a prism like shape rather than the rectangular shape of today's sledgehammers. Thor's Hammer in ancient tradition was depicted similarly to today's club hammer, with a raised center to carry the center of gravity forward along the hammer as shown in Figure 2. Thor's Hammer from historical findings and depictions is often intricately adorned with symbols and references from Nordic mythology, each bearing their own meaning.



Figure 1: A Depiction of a Thor Hammer Pendant Uncovered in Öland, Sweden [1]



Figure 2: Modern Club Hammer Resembling the Traditional Thor's Hammer Shape [3]

Although in the most classical sense Thor's Hammer ought to be defined by its mythological roots, Marvel comic books have over the years revolutionized and breathed new life into the character of Thor and his famous hammer. The Marvel comic series and Marvel film universe depict Thor's Hammer as shown in Figure 3. The hammer is cuboidal, with a straight, seemingly cylindrical handle and leather strap. The edges of the hammer face are beveled, with a perfectly flat face. Some engraving is visible on the hammer, but not as much as on the mythological Thor's Hammer symbol.



Figure 3: Marvel Comic's Hammer of Thor Then and Now. [4] [5]

1.2 Introduction to Design Requirements

In the 2021 Cast in Steel Competition, the Steel Founder's Society of America put forward the challenge to not only produce a steel Thor's Hammer through the use metal casting techniques, but also required the hammer to be fully functional. Furthermore, the hammer was required to weigh a maximum of 6 lbs. and be under 20 inches long. This presents several engineering challenges and requirements which must be considered when designing the casting.

To develop a casting which not only encapsulates Thor's iconic hammer, but is also fully functional, several additional design factors must be considered. First and foremost, Thor's hammer was his weapon of choice and as such it should be fully functional as a weapon of war. The hammer should be strong enough to withstand repeated impact through a variety of materials encountered in battle, including wood, bone, and metal. As such, considerable toughness must be incorporated. Simultaneously, it must be hard enough to resist excessive marring or deformation during use when struck against other objects. For these reasons, the hammer must contain a balance between hardness and toughness to be durable as a weapon.

More than just its effectiveness as a weapon of war, Thor's hammer was also seen as an instrument of blessing in Nordic mythology, and for this reason there should be a sense of elegance and refinement to the implement which goes beyond a mere instrument of war. Thor's hammer should be elegant as well as deadly.

Thus, the design requirements placed upon this product are as follows. First and foremost, the hammer must be made of steel, be under 6 lbs total, and remain under 20 inches long. Second, the hammer must feature a combination of good hardness and toughness to allow for its functionality as an instrument of war. Thirdly, the implement must be aesthetically pleasing and fitting in its symbolic role as an instrument of consecration.

1.3 Introduction to Bimetal Castings

Selection of an alloy for casting applications is often a compromise between mutually exclusive material properties. Applications requiring both high toughness and high hardness often lead to significant compromises because high hardness is advantageous for wear resistance but can result in a brittle material with low toughness. [6] For this reason, the possibility of choosing two alloys whose combined strengths overcome their individual weaknesses is extremely beneficial. This is often accomplished by welding or mechanical fastening; however, both processes add time and cost to the manufacturing process. Recent work done in the field of metal casting has shown that two alloys may be fused through the casting process to form a bimetallic composite featuring a strong, seamless metallurgical bond.

In research done in the area of metal casting for high wear applications, it is shown that cast iron poured on monolithic or crushed steel wear plates offers significant potential for forming cost effective wear components. According to a study performed by T. Wróbel, bimetal casting is an extremely economical means of producing a casting with good surface properties when the interior properties of the casting are unimportant. [7] Figure 4. shows a schematic reproduced from Wróbel's work which demonstrates the principle of bimetal casting, in which a surface alloy was selected for wear performance or high hardness, while the interior of the casting was designed to meet a separate set of criteria. [8]

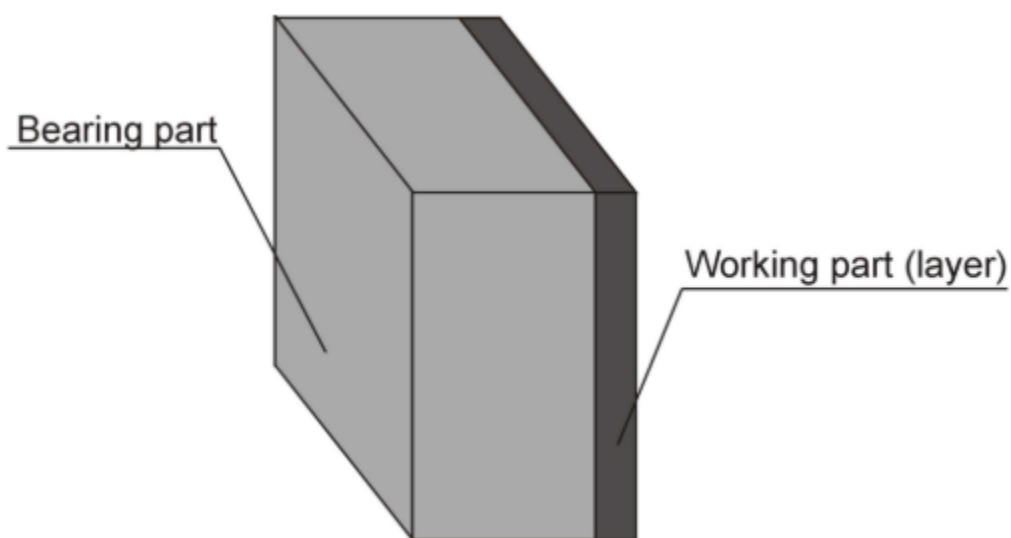


Figure 4: Design Schematic of a Bimetal Casting Reproduced from Work Published by T. Wróbel [8]

In further studies performed on bimetallic castings, it was shown that a bimetals hammer could be cast for industrial crushing applications. This casting featured a crushing surface of high chromium white iron for good wear resistance and a base of low carbon steel for high toughness. This was accomplished by first pouring white iron and allowing it to partially solidify before following up with a second pour of low carbon steel. Figure 5 shows the schematic of such a casting, complete with microstructure analysis and a hardness gradient across the interface region. [9] This study shows the potential for implementing bimetallic casting techniques in the development of a cast hammer for high impact applications.

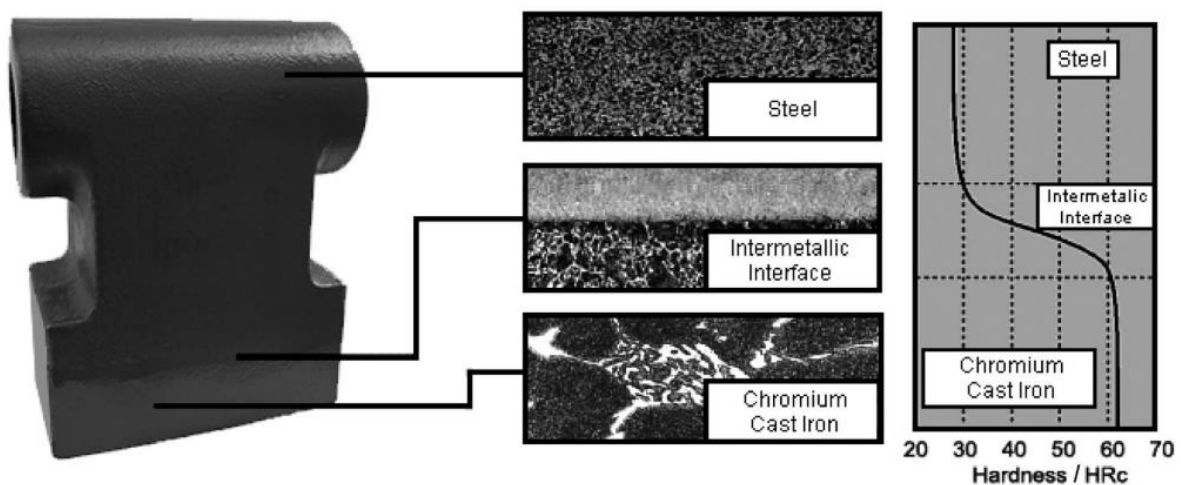


Figure 5: Bimetallic Hammer Cast for Crushing Applications [9]

2. Design and Development

2.1 Designing Thor's Hammer

First, as previously discussed, Thor's hammer features a large, almost oversized head and undersized handle regardless of the overall form factor or specific design adopted. To cast a hammer which is undeniably recognizable as Thor's iconic hammer, the overall size and scale of the hammer cannot be compromised. However, to keep the hammer under 6 lbs., significant design changes must be made. Only three aspects of the hammer may be changed to reduce overall weight. Weight can be reduced by changing the material, the size, or the shape of the casting. However, as the competition specifically requires the hammer be made of steel, weight reduction through alloy change is limited. Although a filler material or other alloys may be used in addition to steel, the core features making the structure a hammer should be steel to be in accordance to the spirit of the competition. The size of the hammer can arguably be changed to some extent to minimize weight, but any significant size reduction would

sacrifice the iconic size which distinguishes Thor's hammer. Lastly, the shape may be changed or modified through optimization methods to reduce the amount of material used within the same form factor. It was the latter method which was adopted for this hammer design, as the overall volume of the classic Thor's Hammer may be retained while internal material which is unimportant to the performance of the hammer is removed.

To accomplish the weight reduction by shape optimization, it was decided that a lightweight structure should be developed which compensates for the center region of the hammer while leaving the faces unaffected. In this manner, the functionality of the hammer face is unchanged but the overall weight is reduced dramatically.

Next, it was decided that a hardened surface was necessary for good hammer performance and resilience but should be supported by a core featuring excellent toughness. The hammer face should be hard, but not so hard that it is prone to cracking when striking metal or bone. For this reason, a surface hardness of between 40 and 50 RHC was targeted. The hammer core should be left unhardened and ductile to improve the toughness of the hammer. This combination between surface hardness and interior toughness will allow the hammer to truly serve as a weapon of war, capable of striking wood, bone, or even steel with impunity.

2.2 Lightweight Structure Design

In order to reduce the overall hammer weight while retaining the classic form factor attributed to Thor's hammer, it was necessary to incorporate a lightweight structure into the casting. A lattice structure was selected as the lightweight structure because they show greater weight reduction potential compared to other optimization methods such as topology optimization without compromising strength. [10] Furthermore, lattice structures are particularly well suited to lightweight components undergoing high impact or compressive loads. Lattice structures show high stiffness coupled with excellent energy absorption while also maintaining excellent strength to weight ratios. [11] For the purpose of this application, a periodic lattice structure was selected which featured repeated unit cell structures whose mechanical behavior is easy to predict through element approximation techniques. [12] In one study comparing a selection of common unit cell lattice morphologies, it was found that tetrakaidekahedron unit cell structures (Shown in Figure 6) significantly outperformed other structures in mechanical testing. [10]

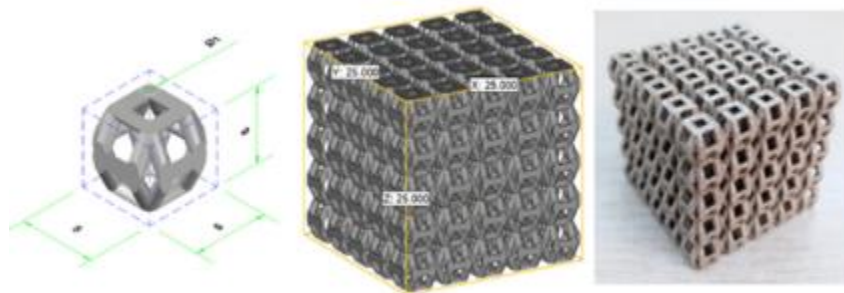


Figure 6: Tetrakaidekahedron Unit Cell Structure [10]

Furthermore, the tetrakaidecahedron unit cell structure also features minimal surface area coupled with other space-filling polygons and is therefore commonly used to approximate ideal grain growth morphology in materials science. [13] The specific grain structure approximation is known as the Kelvin Tetrakaidecahedron. [13] It was for these reasons that the Kelvin tetrakaidecahedron was selected as the unit cell structure to construct the lattice support structure for the lightweight hammer. Such a unit cell structure shows improved mechanical properties in both compression and tension loading, while also paying tribute to materials science by closely approximating the ideal grain structure of steel.

2.3 Alloy Selection and Bimetal Casting Design

For casting the main hammer structure, a combination of excellent toughness and good hardness is required to withstand repeated impact loading without excessive marring of the hammer face. Achieving good hardness may be achieved through increased the carbon content, however increased carbon also results in brittle behavior at room temperature and increases the likelihood of cracking during heat treatment or testing. [14] For this reason, a medium carbon steel should be selected to obtain adequate hardness while avoiding brittle behavior.

Hardenability, or the ability to through harden the material, is also an important factor to consider for developing a good hammer casting. For this application, the hammer face should be able to be hardened through the surface and well into the face of the hammer to prevent excessive deformation. However, the hardenability should be moderate, and should not proceed to far into the casting else the toughness of the material will be negatively affected. According to the ASM Handbook "Steel Selection for Hardening," Ni, Cr, and Mo each increase hardenability modestly. Ni particularly increases hardenability while also increasing toughness through solid solution strengthening. [14] For this reason, a medium carbon Ni-Cr-Mo steel alloy was targeted. 8630 steel is a low-alloy Ni-Cr-Mo steel which shows exceptional toughness, adequate hardness, and good hardenability. The 86xx alloy family was chosen over the commonly used 43xx series as 86xx alloy features lower nickel and meets the required specifications in a more economical manner. 8630 steel was chosen because its medium carbon content helps prevent brittle behavior while the Ni-Cr-Mo content increased toughness and hardenability.

For casting the lattice structure, several unique limitations exist. First, the alloy used to cast the lattice must possess excellent fluidity at thin wall sections. Additionally, tri-junctions occur in the unit cell where three struts diverge from a single point. This tri-junction will favor the formation of porosity due to its higher thermal modulus compared to the struts. Porosity at these locations would severely hinder the mechanical performance of the lattice and should be avoided. Lastly the material must possess high toughness and ductility to allow for elastic deformation and energy absorption during impact loading. While certain grades of steel would provide the fluidity necessary to fill the lattice structure, significant shrinkage porosity would form at the trijunctions due to the solidification shrinkage of steel.

Ductile Iron, on the other hand, provides excellent fluidity at thin wall sections while maintaining ductility. [15] The formation of nodular graphite in the iron matrix also mitigates the formation of shrinkage porosity as the growth of lower density graphite counterbalances the iron matrix shrinkage contraction. A 60-40-18 ductile iron composition is used in many applications and was selected as the target composition for the cast iron lattice because of its excellent elongation and potential to absorb impact.

Table 1: Alloy Selection Overview

	Lattice	Hammer
Material Selection	60-40-18 Ductile Iron	8630 Steel
Key Advantages	Fluidity, Ductility, Minimal Shrinkage	Good hardness, Hardenability, Toughness,

The most important factor however in determining the alloy selection is the interaction between the two metals at the bimetal interface. The liquid metal must retain sufficient heat upon contact with the lattice material that the solid lattice material will partially melt and fuse with the steel casting. In comparing the two selected alloys, 8630 Steel features a solidus temperature well above the solidus temperature of 60-40-18 Ductile Iron as shown in Figure 8 and 9. In Figure 8, the steel will become fully solidified as austenite at approximately 2640 °F (appr. 1450 °C). In Figure 9, Ductile Iron has a solidus temperature of 2120 °F (1170 °C). For this reason, it can be expected that upon casting, the steel will partially remelt and bond with the ductile iron to form a robust bimetal interface. In addition, it is expected to form carbide at the interface when the remelted ductile iron solidifies. As a result, special heat treatments will be required in subsequent processes as described in section 2.7.

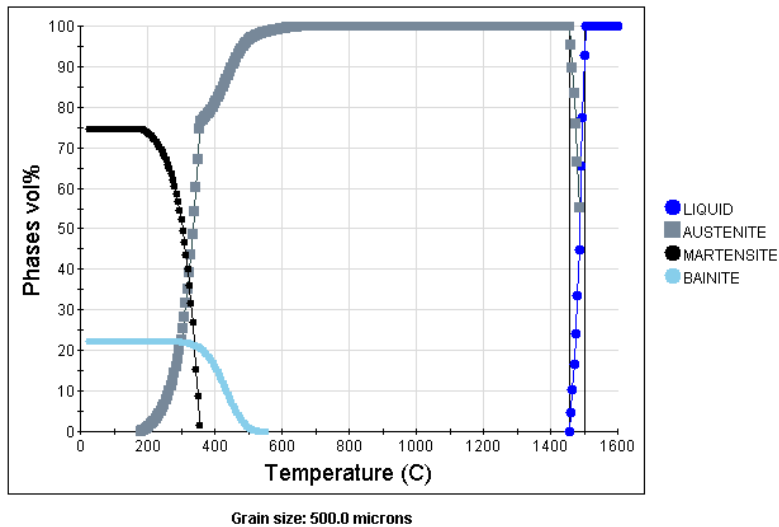


Figure 8: 8630 Steel Equilibrium Phase Transformation Plot

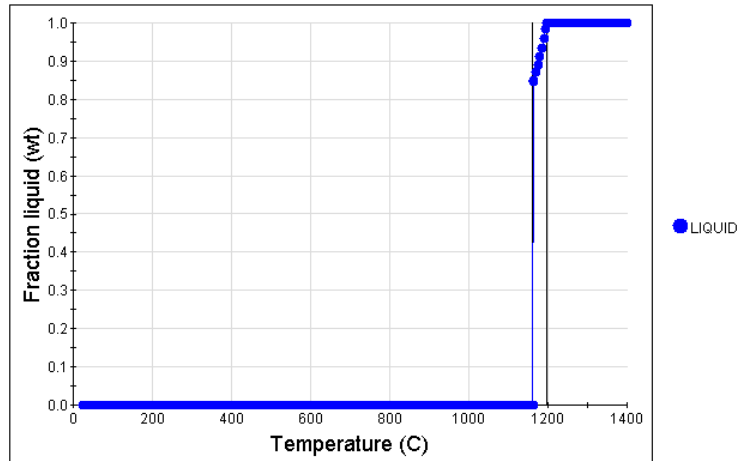


Figure 9: Ductile Iron Equilibrium Solidification Curve Plot

2.4 Hammer Structural Design

The main hammer structure was developed based on the iconic Marvel Universe adaptation of Thor's hammer; however, the middle portion of the hammer was removed to reduce weight. Nonetheless, the hammer faces and the hammer eye were retained from the original design. The faces and hammer eye were connected by a diamond beam cross section, shown in Figure 10. This was designed to be thick enough to allow for adequate liquid flow during casting but not so thick that unnecessary weight was added. The hammer face was designed to be $\frac{1}{4}$ " thick, which was selected based on the hardenability chart for 8630. [16] A minimum hardness of 40 HRC is possible up to $\frac{1}{4}$ " from the quench surface when the hammer is face quenched. For a through hardened hammer face, $\frac{1}{4}$ " thickness was desirable.

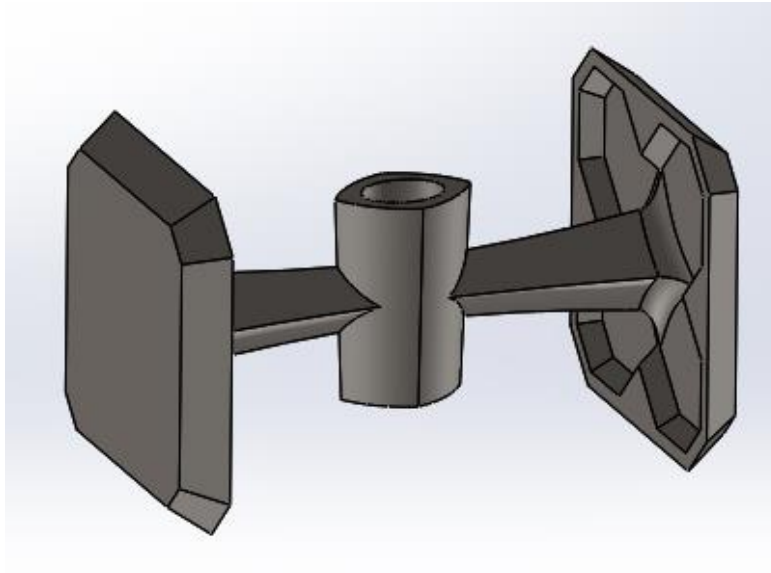


Figure 10: Hammer Structure Design

The hammer eye was designed dimensionally based on a standard blacksmithing hammer handle featuring an oval eye. A 1° taper was added to the eye as shown in Figure 11, allowing for a secure handle fitment through a kerf-and-wedge process. This process is demonstrated in Figure 12, drawn from a publication of the Blacksmithing Organization of Arkansas. [17]

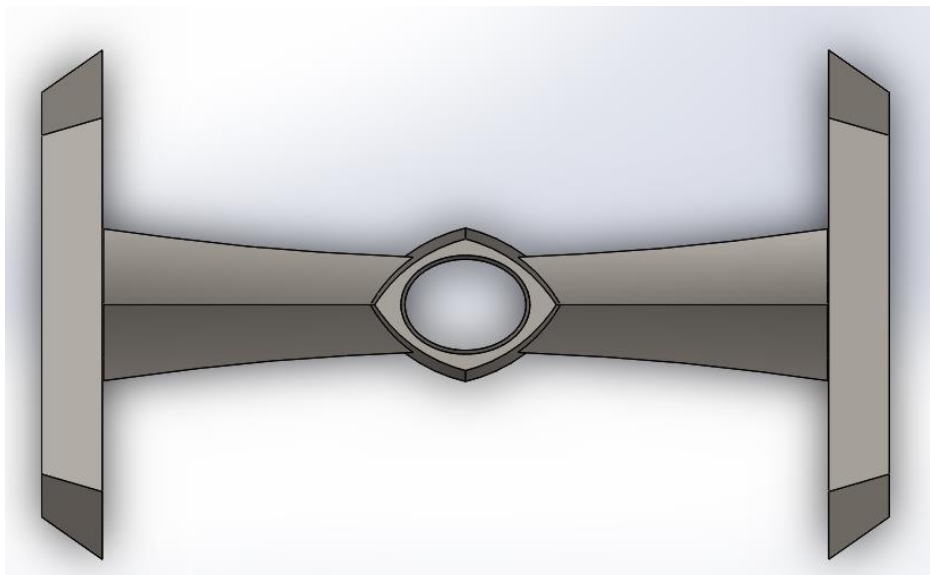


Figure 11: 1° Taper Added to Hammer Eye

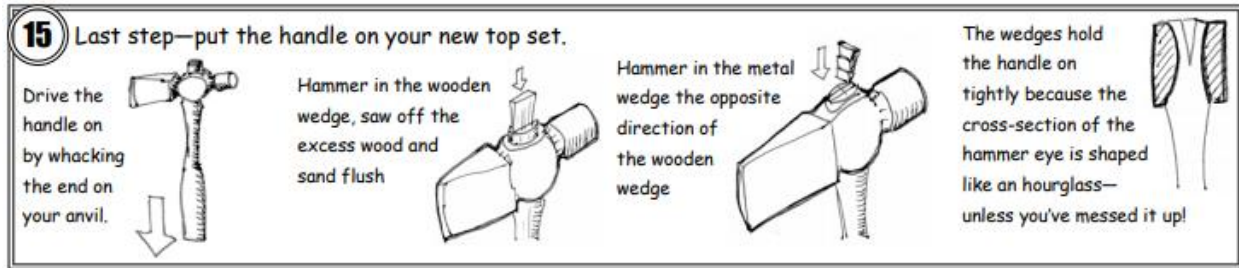


Figure 12: Proper Handle Mounting Procedure for Blacksmith Tools [17]

Lastly, features were included on the backside of the hammer face to allow for full contact between the lattice and the hammer structure, as shown in Figure 13. Built-up triangular extrusion features meet precisely with the faces of the lattice structure. This not only gives the lattice structure something to mount to but also increases the thermal modulus of the casting at these key locations to allow for proper melting and fusion of the ductile iron lattice.

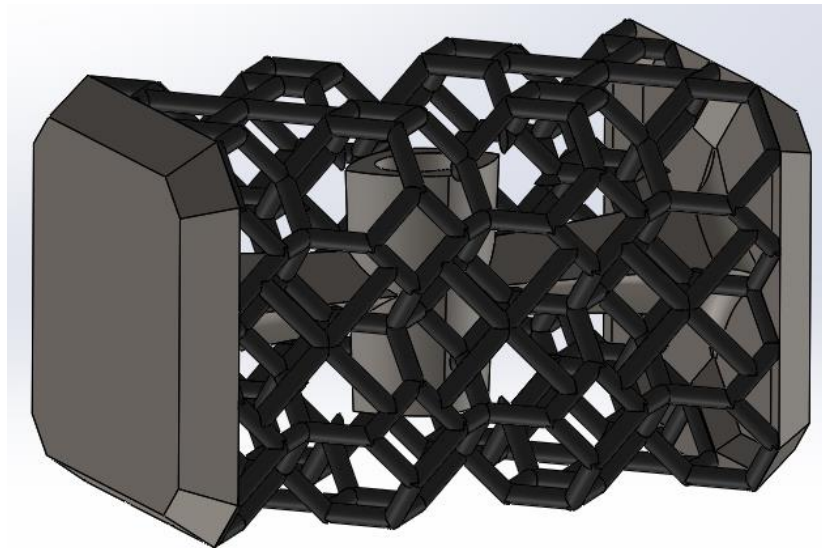


Figure 13: Tetrakaidecahedron Lattice Fitted to Hammer Structure

The lattice structure serves another purpose relating to the hammer structure. Because the beam supporting the hammer faces is connected in the center of the face, excessive moment loads could develop when the hammer is struck on the edges or corners of the faces. Because the lattice structure connects to the hammer face around the edges and corners, it will resolve any moment load which would otherwise be generated as well as absorb impact energy generated by sharp contact to the edges of the hammer.

2.5 Casting Process Selection and Design

To cast the complex geometry of the lightweight structure, the investment casting was an obvious fit. Investment casting offers the ability to capture intricate details, produce thin wall castings, and maintain excellent surface finish. [18] Additionally, investment casting allows for high mold preheat temperatures (between 1600 and 2000 °F for ferrous alloys) to aid in complete filling of intricate designs. [18] Although investment casting is significantly more labor intensive than other casting methods and increases manufacturing cost in a commercial sense, investment casting is capable of producing castings which are unattainable other means. Additionally, the improvement in surface finish and design complexity often more than make up for the increase in production cost. For these reasons, investment casting was selected as the casting method for producing the lightweight ductile iron lattice structure.

For the main hammer structure, sand casting was selected as the casting method. Although the casting of the hammer structure required some unique engineering solutions to accommodate the lattice structure, the overall design primarily featured standard geometries which are easily castable through sand casting methods. The internal cavities and lattice features can be accommodated by a sand core built around the lattice structure. High surface finish was not necessary for the interior of the hammer, and the hammer faces would require polishing regardless of the casting method, so surface resolution was not a primary concern in the selection of the casting method. For this reason, sand casting was selected as the production method for the hammer structure.

2.6 Gating and Riser Design

MAGMA was used to validate the castability of the proposed design as well as to develop an appropriate feeding system for the casting. The ability of the bimetal casting to properly fuse and form a strong interface was evaluated based on MAGMA simulation thermal analysis data. Filling temperature simulations were also used to verify proper filling of the casting. Lastly, porosity was predicted through simulation and accounted for by riser placement. Separate simulations were prepared for each stage of the two-step casting process. First, the investment cast ductile iron lattice was simulated to verify castability, determine appropriate pouring temperature, and determine the minimum preheat temperature. Second, the steel hammer structure was simulated with the lattice chill feature incorporated. These simulations together predicted the overall outcome of the casting process.

The ductile lattice casting was simulated using the investment casting module of MAGMASoft®. GJS-400 Ductile Iron Alloy was selected from the MAGMA database for simulation purposes. A top-down gating approach was adopted to achieve maximum head pressure for complete filling, as shown in Figure X. A Foseco 2.5"x6" Kalpur sleeve was used in the simulation to serve as an insulated downsprue-riser hybrid. Important MAGMA simulation parameters are presented in Table 2. Pouring time was calculated using Equation 1 based on the combined weight of the casting and gating system (W) in lbm, with the wall thickness coefficient (S) being 1.63. [19] The wall thickness coefficient was selected based on established standards for a thin casting wall thickness according to published data. [19]

Equation 1:
$$t = S\sqrt{W}$$

Table 2: Lattice Simulation MAGMA Parameters

Critical Parameters	Value	Unit
Casting System Weight	4.36	lbm
Pouring Time	3.4	sec
Shell Thickness	10	mm
Pouring Temperature	2550	°F
Shell Preheat Temperature	1750	°F
Simulation Alloy Selection	GJS-400	

A pouring temperature of 2550 °F (approx. 1400 °C) combined with an investment shell preheat of 1750 °F (950 °C) was chosen to maintain fluidity through the thin wall sections. From the MAGMA database for GJS-400 Ductile Iron, the liquidus temperature for the material was 2135 °F (1168 °C). After simulation, it was determined that the minimum temperature during filling was 2183 °F (1195 °C) as shown in Figure 14, and therefore the mold could be expected to fill completely.

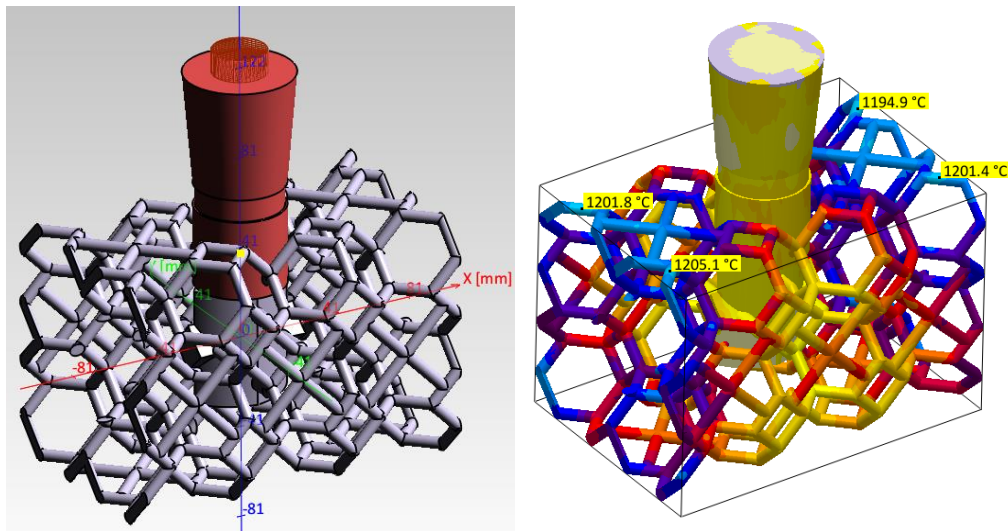


Figure 14: MAGMAsoft® Investment Cast Lattice Gating

Following the finalization of the lattice filling simulation, a green sand casting simulation was developed for the steel hammer casting. The Ductile Iron Lattice was included in this simulation and specified as a GJS-400 iron Chill. The steel casting alloy selected for this simulation was 4340 steel from the MAGMA database. A Fosco Kalpur sleeve was added to the hammer eye structure and used as an insulated downsprue and top riser combination. Risers were added to either end of the casting to feed the hammer faces. One vent was added to the top of each hammer face to accommodate for low permeability in the chemically bonded sand. A The final gating and riser system is shown in Figure 15. Simulation parameters are shown in Table 3. Furan sand was selected as the mold material. The pouring

time was once again calculated according to Equation W, however this time a larger wall thickness coefficient of 1.85 was selected. [19]

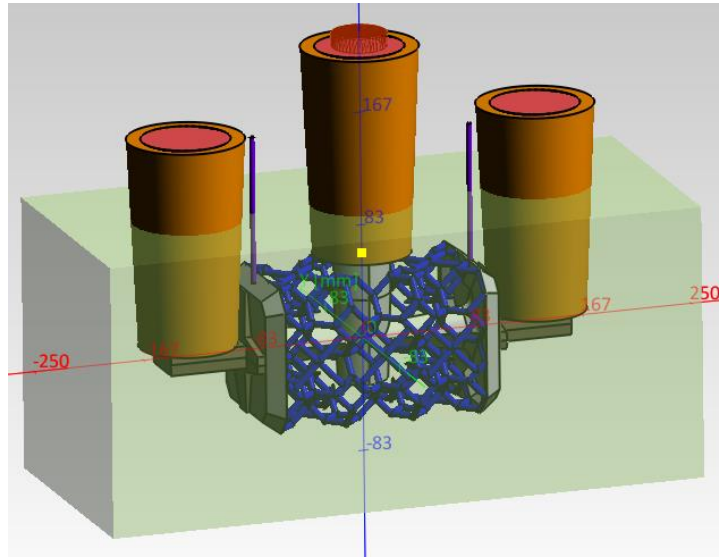


Figure 15: Gating and Riser Design for Bimetal Hammer Casting

Table 3: Hammer Structure MAGMA Parameters

Critical Parameters	Value	Unit
Casting System Weight	23.15	lbm
Pouring Time	8.9	sec
Sand Material	Furan Sand	
Pouring Temperature	2912	°F
Mold Temperature	80	°F
Simulation Alloy Selection	4340	

From the MAGMA Simulations, the temperature profile of the casting was obtained to predict the filling behavior of the casting, but also to predict the ability of the lattice to fuse with the steel casting. From the temperature profile shown in Figure 16, the temperature of the liquid steel casting at the surface of the lattice structure is shown to be well above the liquidus temperature of ductile iron and therefore the two materials together should weld fully together.

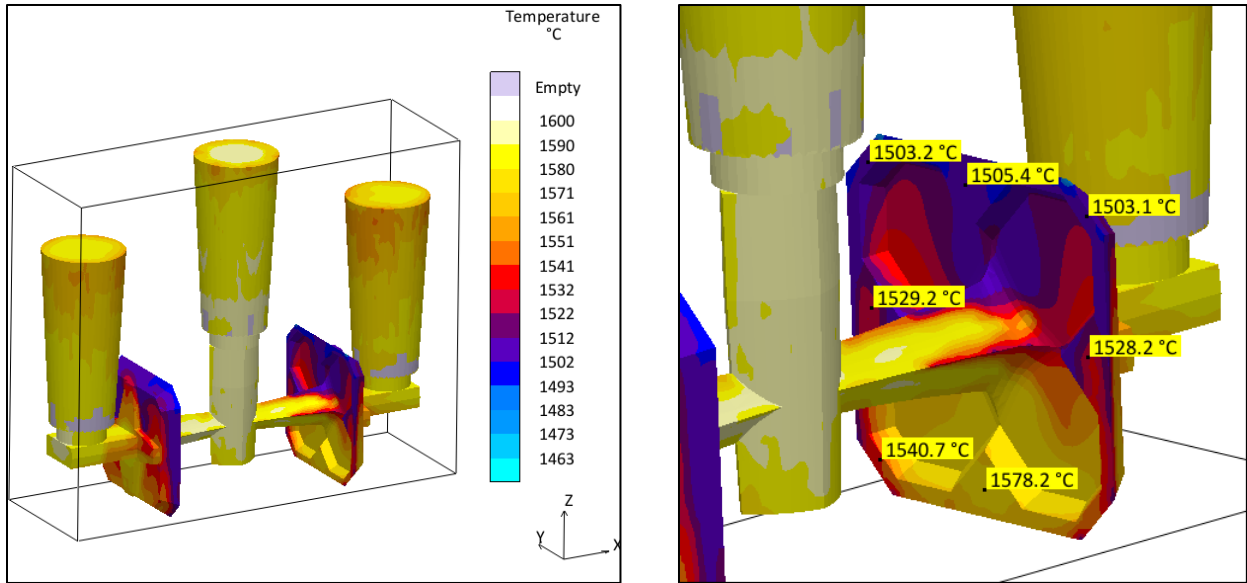


Figure 16: Steel Casting Temperature Profile

The MAGMA simulation results were also used to predict the severity of porosity in the hammer face. It was found that negligible porosity defects were predicted to occur in the casting. The MAGMA porosity simulation results are shown in Figure 17. A cross shaped facial feature was added to the hammer face to prevent porosity from forming at the points of increased thermal modulus discussed in the hammer structure design.

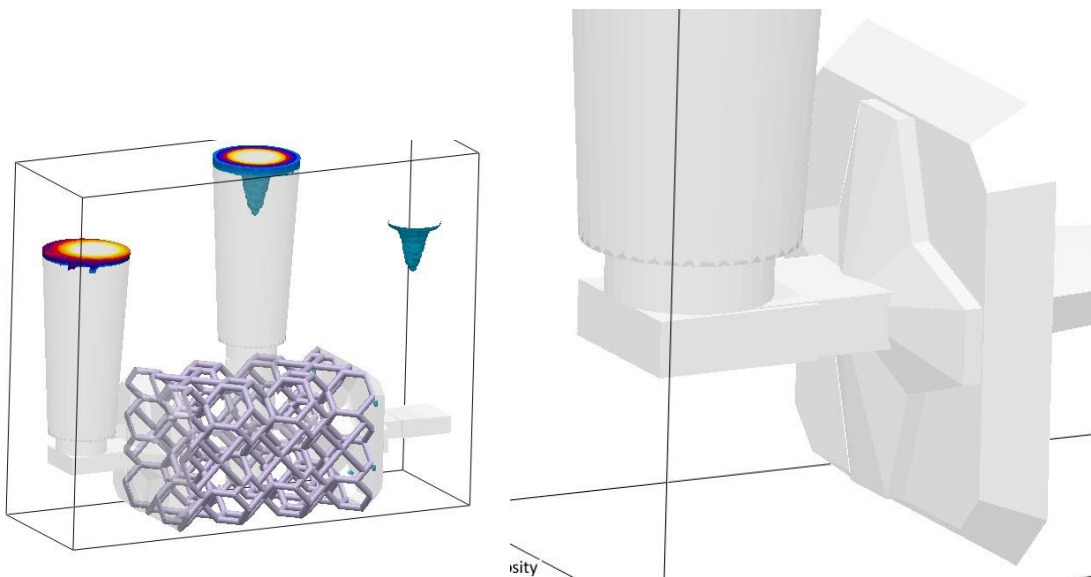


Figure 17: Porosity Analysis of Bimetallic Hammer Casting

2.7 Heat Treatment Design

Prior to the design of the heat treatment procedure, the chemistry of the two alloys used were obtained through spectrometry. These are reported in Tables 4 and 5 in section 4.1. The exact chemistries were used to generate cooling curves using JMatPro thermodynamic calculation software. Continuous Cooling Transformation (CCT) curves were obtained and used to predict the microstructure response to various heat treatment procedures.

A normalizing procedure was first designed to relieve internal stresses within the casting and to refine the grain structure. According to data published in the ASM handbook for heat treatment of low alloy steel, the recommended normalizing temperature for 8630 steel is 1650 °F. [16] When normalizing, the component should be held for approximately 1 hour per inch to bring the entire casting up to the normalizing temperature. The part should then be removed to air cool to ensure the relief of residual stresses while simultaneously refining the grain structure.

Although the normalizing heat treatment was specifically selected from recommendations for 8630 steel, this process is also highly beneficial to improving the mechanical properties of the ductile iron lattice. According to the ASM handbook “Heat Treating and Properties of Ductile Iron”, normalizing is beneficial to most ductile iron castings, generally resulting in a fine pearlitic matrix. [20] This does, however, largely depend on the alloy composition. Using CCT curves generated by JmatPro for the measured Ductile Iron chemistry and shown in Figure 18, an average air-cooling rate should produce a fully pearlitic matrix in the Ductile Iron. For this reason, the selected normalizing cycle was identified as being beneficial to both alloys in the bimetallic casting.

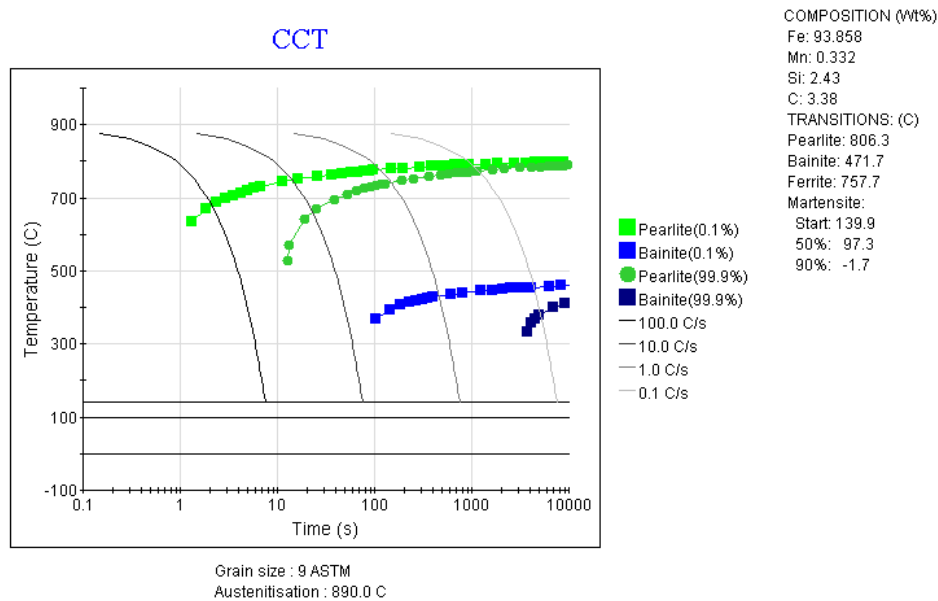


Figure 18: CCT Curve Generated from Measured Ductile Iron Chemistry

When the final hammer structure was cast, samples were taken for the purpose of designing and validating a heat treatment procedure. A ductile iron sample was taken from the cast iron lattice and inserted into a separate mold for the purpose of analyzing the bimetal composite interface and the resulting microstructures of each alloy. This sample was then cut, polished, and prepared for metallography examination. A tight metallurgical bonding was observed at the interface, as shown in Figure 19.

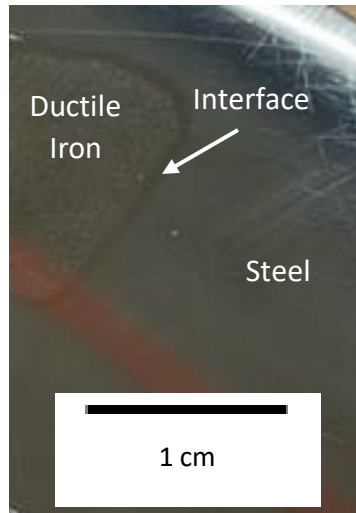


Figure 19: As-Cast Sample Specimen for Analysis of the Bimetal Interface

From the as-cast microstructure, several key insights were gathered which aided in designing a heat treatment procedure. Metallography images of the bimetal interface show a solid interface region. In Figure 20, a low magnification image of the interface region between the steel (right) and cast iron (left) is shown. From this image however, it is abundantly clear that the rapid remelting and solidification of the ductile iron resulting in carbide formation from the metastable eutectic transformation. The metastable eutectic reaction is a controlled by cooling rate, nucleation potential in the melt, and alloy content. [21] Because the ductile iron has been remelted, there will not be enough inoculant present to nucleate graphite. Additionally, the fast melting and re-solidification rates will further favor iron carbide formation due to higher undercooling. [21] This bimetal casting resulted in white iron forming in the weld zone. A higher magnification image of the carbides resulting from this process is shown in Figure 21.

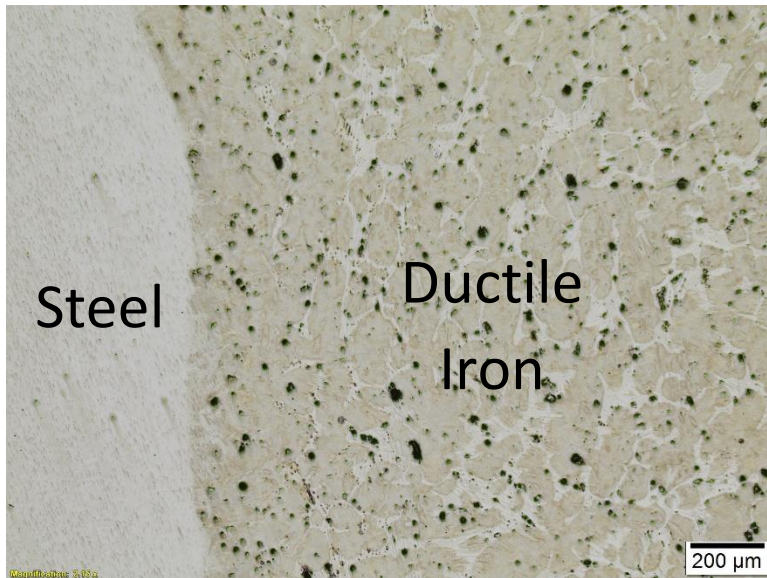


Figure 20: Low Magnification Image of Bimetal Interface Region

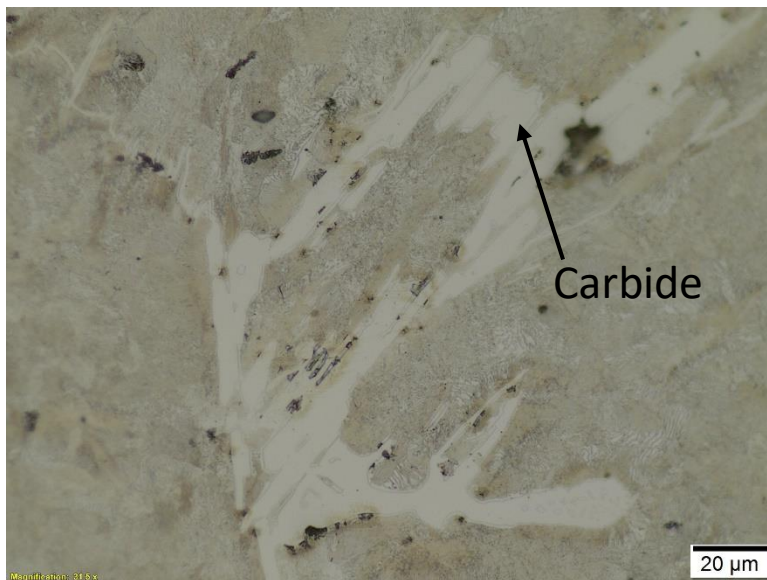


Figure 21: High Magnification Image of Carbides Formed in the Cast Iron

White Iron forming at the bimetal interface would be severely detrimental to overall mechanical performance as it forms and propagates along the iron carbide plates, resulting in brittle behavior. For the hammer to adequately withstand high impact loading the presence of iron carbide must first be eliminated. For this reason, a malleable iron heat treatment procedure was adopted. This heat treatment procedure was designed based on documentation from ASM handbooks on malleable iron heat treatment as well as advice offered by Dr. Mingzhi Xu of Georgia Southern University and Dr. Von L. Richards of Missouri S&T.

To begin the malleable iron heat treatment, the casting should be first held at 700 °F for 2 hrs. to facilitate nitride precipitation. This step is important to allow for a nucleation site for graphite to grow as the iron carbides are dissolved. Following nitride precipitation, the casting should be brought to 1750 °F for first stage graphitization. [22] In this stage, iron carbides are dissolved, and malleable graphite is formed. The casting was held at this temperature for 6 hrs to allow for maximum dissolution of the iron carbides.

One principal concern during this step was undesired grain growth in the steel portion of the casting. However, because the steel chemistry contained 0.03 wt% Al, it can be expected that AlN will have formed during the casting process. This nitride is a strong grain pinning agent, with a solubility well above the proposed first stage graphitization temperature when calculated based on 0.03 wt% Al and an estimated 90 ppm N. The equation to determine the solubility of AlN is shown in Equation 2, and provided that the temperature remains under the solubility limit AlN will remain precipitated out of solution and will prevent significant grain growth in the steel. [23]

Equation 2:
$$\log_{10}([Al][N]) = \left(\frac{-6770}{T(^{\circ}C)} + 1.03 \right)$$

After the completion of first stage graphitization, the casting should be removed and allowed to air quench to near 1365 °F. Second state graphitization is then initiated by placing the casting immediately in a furnace already held at 1365 °F. The furnace should be then shut off and the casting allowed to slowly cool through the allotropic transformation range in the iron. This obtains an iron matrix completely free of carbides. [22] Figure 22 provides the heat treatment cycle designed for the malleable iron transformation.

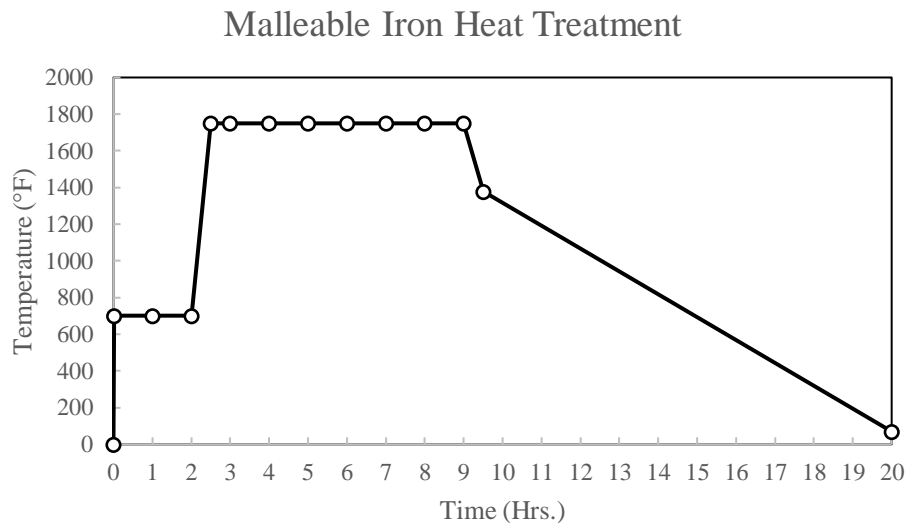


Figure 22: Malleable Iron Heat Treatment Cycle Designed for the Hammer Casting

Following the malleable iron treatment, a Quench and Temper process (Q&T) was designed for the purpose of hardening the hammer of the faces. In doing so however, the hammer surface must harden while leaving the remainder of the casting ductile. To accomplish this, the lattice structure should be well insulated from the casting, and the quench media should contact only the hammer faces. The quench process was designed according to published data for 8630 steel available in the ASM handbook for heat treating of low alloy steels. [16] According to this source, Oil, polymer, and water are all appropriate quench media for 8630 steel. [16] In order to achieve a hardened surface, a severe quench is necessary to avoid ferrite formation according to the CCT diagram produced for the given 8360 alloy chemistry. According to the CCT diagram shown in Figure 23, the surface should be brought from the austenizing temperature of 1630 °F (approx. 890 °C) to the martensite start temperature in under 10 seconds to achieve a primarily martensitic microstructure mixed with bainite. For this reason, water was selected as the appropriate quench media to obtain the desired surface quench rate.

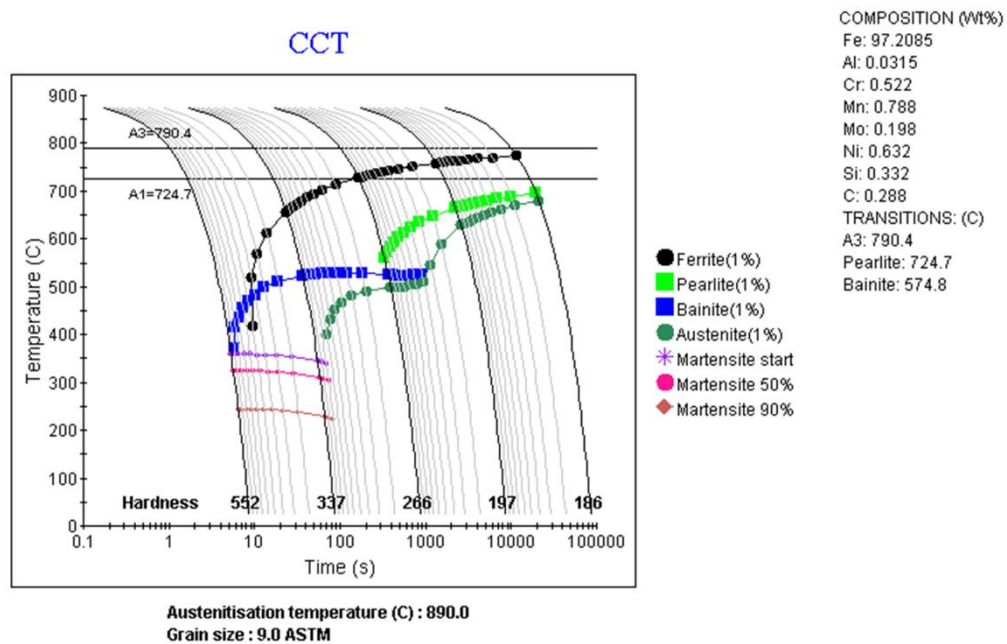


Figure 23: CCT Diagram for 8630 Steel Produced by JMatPro

Lastly, a temper process was designed to improve the overall toughness of the hammer face. According to the ASM heat treatment handbook for low alloy steels, 86xx alloys respond similarly to 43xx series alloys of similar carbon content. [16] For this reason, it can be expected that the temper response of 8630 would be similar to that of 4340. In a thesis published regarding 4340 steels for use in ground engaging tools, an impact energy versus tempering temperature chart was presented and is reproduced here in Figure 24. As shown in this figure, for stage 1 tempering, maximum toughness was achieved at 200 °C. [24] For this reason, a 1 hr. temper at 400°F (approx. 200 °C) was selected to allow for carbon redistribution and transition carbide formation without significantly affecting hardness. [24]

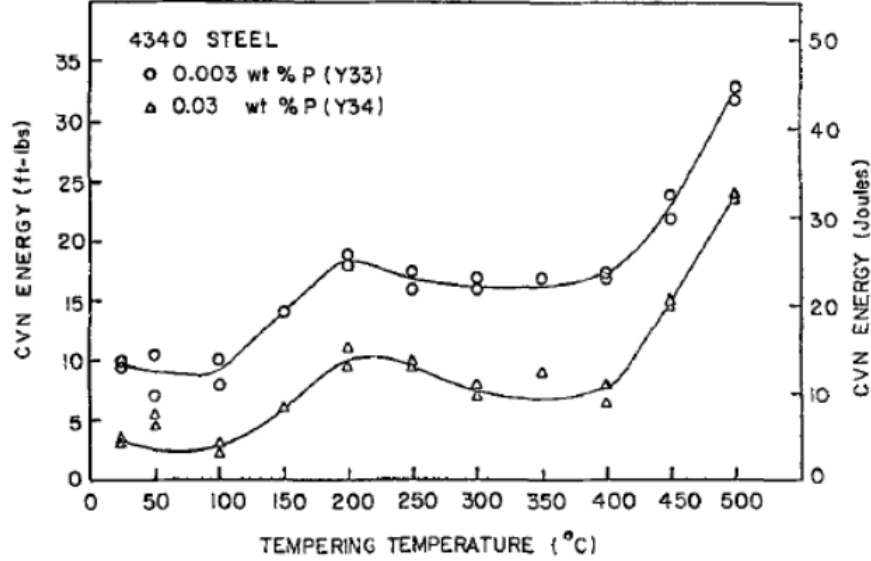


Figure 24: Tempering Temperature versus Impact Energy Chart for 4340 Steel Alloy [24]

3. Manufacturing Methods

3.1 Additive Manufacturing of Patterns

Additive manufacturing was used to produce the casting patterns for both the lattice structure and the hammer casting. Fused Filament Fabrication (FFF) was primarily used in the making of both the expendable investment casting pattern and the matchplate pattern used for casting the steel hammer structure. PolyCast™, a novel investment casting PLA material produced by PolyMaker, was used to produce the lattice structure. The structure was printed with minimal infill to reduce the thermal expansion force experience by the shell. Figure 25 shows the printing in process on a Creality Ender 3 Pro series FFF printer. The printed lattice structure was then smoothed with ethanol to obtain a layer free surface finish.

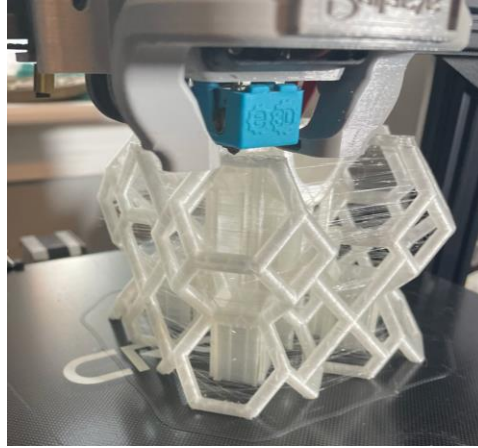


Figure 25: Printing the Lattice Structure on an FFF Printer

FFF was also used to make the patterns for the hammer pattern. The hammer endcap and gating features were 3D printed for mounting to the matchplate pattern. Riser alignment features were included to easily mount Foseco Kalpur insulation sleeves. Additionally, a core box was produced by additive manufacturing. These models were not designed to be expendable, so standard PLA material was used. These components were printed on a Creality CR-10s pro FFF machine.

3.2 Investment Shell Production

The investment casting mold was prepared by repeated coating with a ceramic slurry until a thick shell was obtained. A ceramic slurry was prepared from fused silica flour and colloidal silica binder in a 2 to 1 ratio by weight. Fused silica flour was selected as the refractory for its low coefficient of thermal expansion in fused silica form. [18] At elevated temperatures associated with ferrous casting, fused silica will transform phases into cristobalite, a distinct silica phase which involves a volumetric change which aids in breaking out the shell. Silica stucco was used to reinforce the ceramic shell between layers, with fine mesh fused silica stucco being added to the first two primary coats, and coarse mesh fused silica stuccoing the following backup coats. The primary slurry coats were covered in fine mesh stucco to increase strength without compromising surface finish. Backup coats do not require the same surface resolution but are rather designed to increase the strength and permeability of the mold and therefore much coarser.

According to the Polymaker application guide for PolyCast™, 5-6 backup coats are recommended to prevent shell cracking during burnout. In producing the investment shell for the ductile iron lattice, 2 primary coats were applied followed by 6 backup coats. The final investment shell is shown in Figure 26. The investment shell was allowed to dry for at least 4 hours in between each coat to allow the shell to fully dry. It was then placed in an oven at low temperature (100 °F) for 12 hours to ensure the shell was free of moisture. The shell was then aged for 24 hours in the oven at 270 °F to allow the PolyCast™ pattern to soften and pull away from the mold wall slightly, reducing thermal expansion stress upon burnout. The investment shells were placed in a sintering furnace for 1 hour set at 1560 °F (850 °C) to simultaneously sinter the shell and burn out the PolyCast™ pattern. According to Polymaker, the low ash

content of the patterns eliminates the need for washing prior to casting, and due to the difficulty of removing water from the complex lattice channels, this step was skipped.



Figure 26: Ductile Iron Lattice Investment Shell

3.3 Sand Mold Construction

To produce the sand mold for casting the hammer structure, a matchplate pattern was produced that was designed for use with chemically bonded sand. Because the cope and drag patterns for the hammer casting are symmetrical, only one pattern was ultimately needed. For this reason, a flaskless mold design was adopted so that the same pattern could be used to produce both the cope and the drag. As shown in Figure 27, significant taper was incorporated into the flask to allow for easy mold removal. Wood was used to form the core print for the lattice, and 3D printed patterns for the hammer faces were adhered to the core print. Figure 27 shows the final matchplate pattern, designed to produce a flaskless chemically bonded sand pattern.



Figure 27: Matchplate Pattern for Flaskless Chemically Bonded Sand Mold

Prior to mold packing, the entire surface was coated with a zip-slip coating to facilitate clean removal of the sand mold. The drag was produced by packing chemically bonded sand in the pattern. The sand was allowed to cure for 10 minutes prior to removal. Next, a downsprue alignment feature was attached to the top of the core print block and three Foseco sleeves were attached. One in the center for the downsprue, and two on either side for the risers. Sand was again packed and allowed to cure, then a vent was drilled through the mold for each hammer face. The final cope mold cavity is shown in Figure 28. In this manner, both the drag and the cope of the sand mold were created.

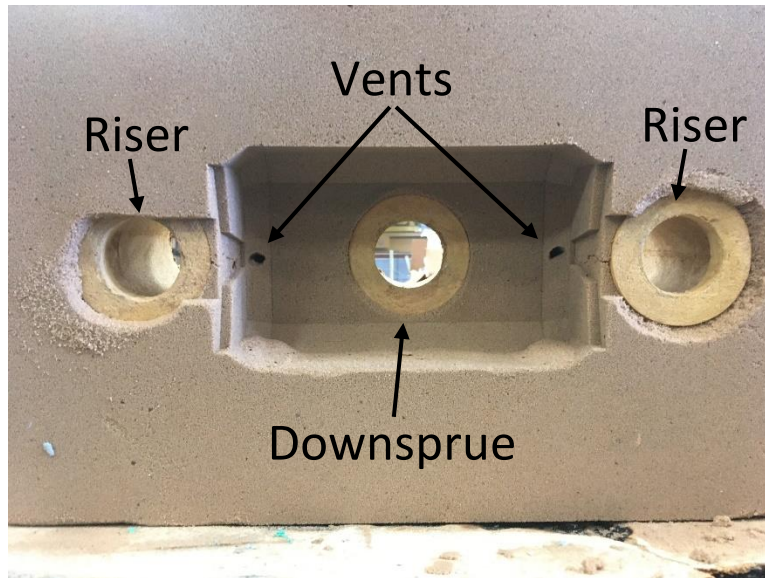


Figure 28: Cope Mold Cavity, Illustrating Downsprue, Vents, and Side Risers

The lattice core was constructed from a three-part system attached to the finished lattice structure. The investment shell was fully removed from the lattice and the downsprue was machined off. The faces were ground perfectly flat to ensure proper bonding between the ductile iron and the cast steel. End caps were attached to either side of the cast iron lattice. Attached to these endcaps was the diamond cross beam structure. The hammer eye feature was placed down in the lattice and the diamond cross beams met and attached with the eye via alignment pins. Ultimately, this formed a removable three-part pattern for the sand core as shown in Figure 29(a). Chemically bonded sand was then carefully packed into the cast iron lattice until the structure was fully infiltrated with sand as shown in Figure 29(b). This was allowed to cure fully before the three patterns were removed. Excess sand was carefully carved off of the sides of the lattice, leaving a final sand core with the internal cavity forming the interior hammer features as shown in Figure 29(c). The end faces of the lattice were left exposed to allow full contact with the liquid steel.

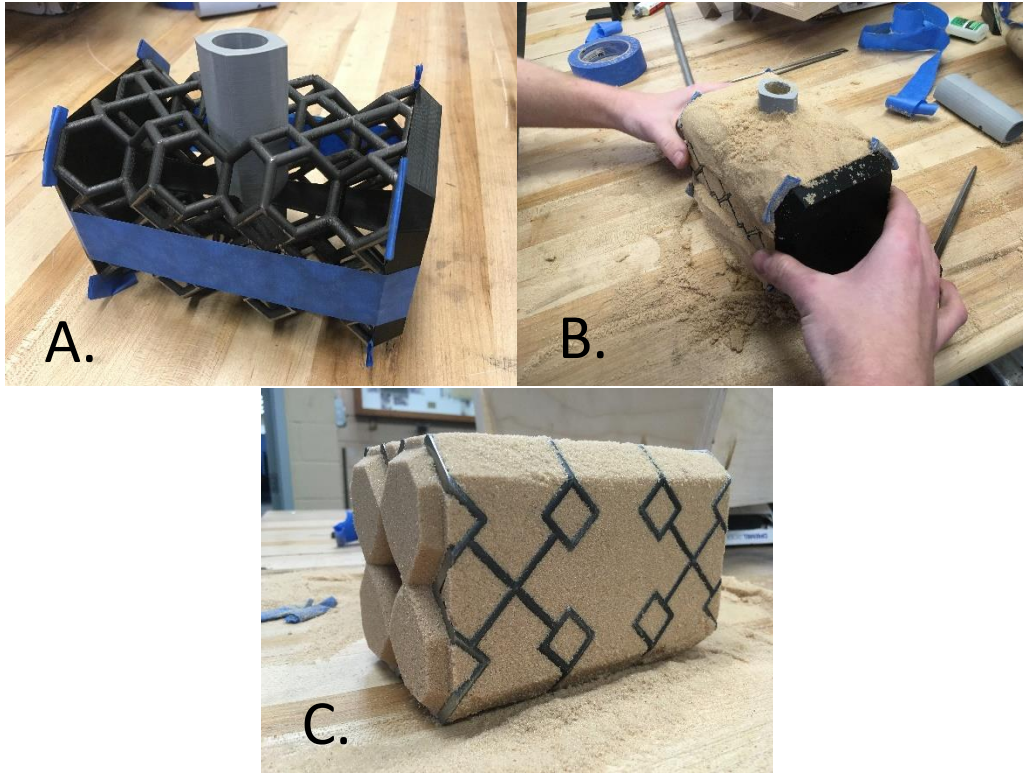


Figure 29: Creation of the Sand Core

Finally, the sand core was carefully inserted into the drag of the final mold and secured using mold glue as shown in Figure 30(b). The two halves were carefully assembled, using the core as an alignment feature. The two halves were sealed with mold glue and the mold was ready for casting. The final mold is shown in Figure 30(a).

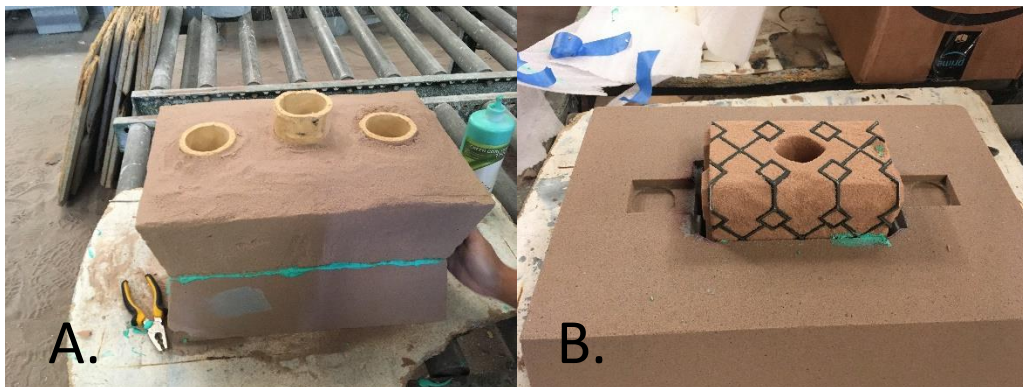


Figure 30: Final Sand Mold (Left) and Internal Iron Lattice Core (Right)

3.4 Casting Process

The final casting of both the ductile iron lattice and the steel hammer was done with the assistance of Carolina Metal Casting as a part of their normal production pour. Both melts were done in an InductoTherm induction furnace, and chemistry samples were obtained from each heat for accurate interpretation of the casting results.

To cast the ductile iron lattice, the investment shell was first preheated to 1850 °F (approx. 1000 °C) to ensure complete filling of the casting. This was removed from the furnace moments before the pour took place and wrapped in kaowool to retain maximum heat. The ductile iron was poured at 2636 °F (approx. 1400 °C). The steel casting was performed with the mold at room temperature. In this case, 8630 steel was poured at 3059 °F (approx. 1680 °C).

3.5 Postprocessing

Following the casting process, postprocessing was performed in the Georgia Southern foundry and machine shop. The final casting was first normalized prior to machining to relieve any internal stresses resulting from the bimetal casting process. Next, the risers and most of the downsprue was cut off using a band saw. The remainder of the downsprue was first drilled out, as shown in Figure 31, then milled off. Additionally, the top and bottom faces of the hammer eye were machined flat. Next, a slot was machined for the hammer eye, and a taper was ground into the feature to allow for the handle to be secured by a kerf-and-wedge method. The faces of the hammer were finished by surface milling to obtain an even surface, and the bevels were ground flat using a belt sander.

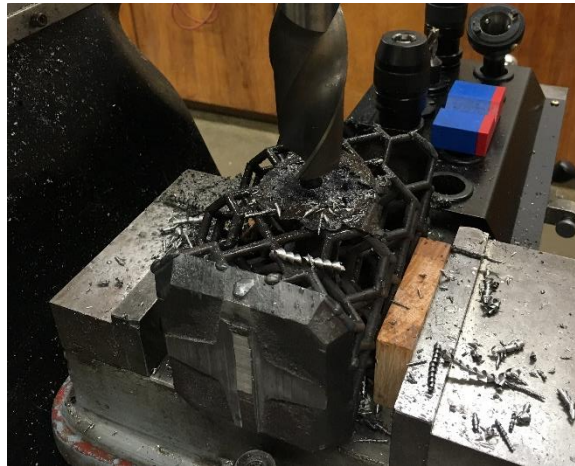


Figure 31. Machining off the Downsprue

Unfortunately, the casting possessed one major flaw which required an additional step of post processing. After the casting had been cleaned up, it was found that the steel casting did not fuse properly to the ductile iron casting in selected regions of higher stress due to the mismatch of thermal expansion coefficient between the cast iron and steel. For this reason, additional welding was required

to complete the casting. MIG welding was used to join the two castings. The entire casting was first preheated in the heat treatment oven to 400 °F. Heat was maintained at localized points with a handheld torch while the lattice was welded to the steel casting. The weld beads were then ground flat to the surface and cleaned up using a rotary tool and grinding stones.

3.6 Heat Treatment

The individual heat treatment procedures were carried out according to the designs adopted for the normalization, malleable iron treatment, and quench and temper processes. One normalization cycle was performed on the casting prior to post processing. Next, after all machining, welding, and major grinding operations were complete, one normalization cycle was performed to prepare the casting for malleable iron heat treatment. Prior to this however the casting was carefully wrapped in steel foil to form an airtight package as much as possible to prevent excessive decarbonization of the casting. The malleable iron heat treatment was carried out, followed by two more normalization cycles to counter any potential grain growth in the steel. Lastly, the quench and temper processes were completed as designed. Prior to the austenization for the quench, the steel foil was removed from the casting and the lattice structure was packed and then wrapped with kaowool to isolate the ductile iron lattice from the quench. Once the casting was at room temperature after the quench process it was immediately placed in a convection oven to temper. The complete thermal processing cycle is shown in Figure 32.

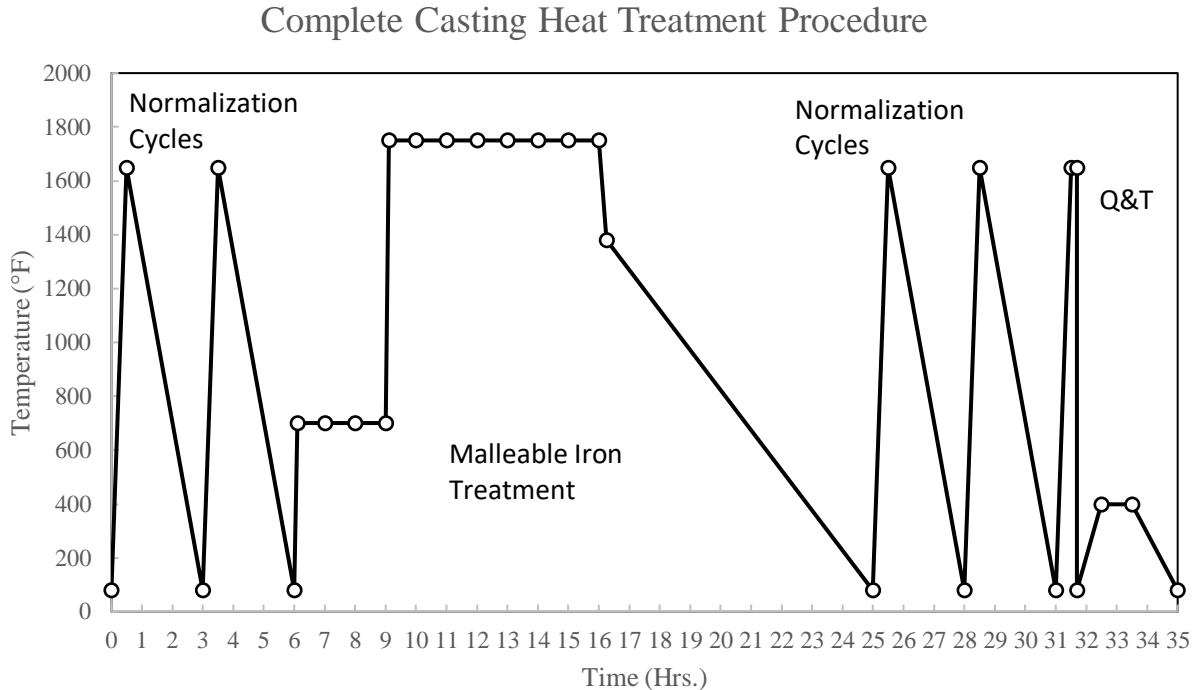


Figure 32: Complete Heat Treatment Procedure Performed on Bimetal Casting

3.7 Final Preparation

Finally, once the casting was completely machined to net shape and the heat treatment process was complete, the hammer was prepared for its final appearance. The casting was placed in a vibratory tumbler to aid in removing the scale and oxides formed on the surface during the heat treatment procedure. It was then thoroughly sand blasted to remove any remaining debris from the interior crevasses of the lattice. Next, to prevent the cast iron lattice and interior low alloy steel from rusting, the lattice and interior of the casting was seasoned in a manner similar to that used on cast iron cookware. Spray oil was applied to the interior of the casting and it was placed in a convection oven at low heat. This was repeated several times to allow a thick seasoning coat to form, giving the interior of hammer an appealing matte black texture while simultaneously preventing unwanted oxidation. The faces of the hammer and the sides of the lattice were then polished using a buffing wheel and buffing compound until a near mirror finish was achieved. A total mirror finish was not targeted as this would amplify any scratches which will form over the usage cycle of any hammer implement.

A hickory engineer's hammer handle was sourced from a blacksmithing equipment supplier and customized to fit the hammer weight and size. An oval handle cross section was selected to prevent the hammer from twisting or sliding easily in the operator's grip. The handle was shortened to improve the overall balance and fitted to the hammer eye. Goatskin was hand tooled to provide extra texture and grip security, then was wet molded to match the hammer handle profile and laced in place. Decorative Turks head knots were added above and below the grip to provide both a firm hand stop and to improve the overall aesthetic. The final hammer handle is shown in Figure 33.



Figure 33: Handle Wrapped in Wet Molded Hand-tooled Goatskin and Finished with Turks Head Lacing

Lastly, the hammer was mounted to the handle through a kerf-and-wedge process. After the handle was fitted snugly to the hammer eye using sandpaper, two perpendicular kerfs were cut into the handle. The handle was installed firmly into the hammer, and wedges were pounded into the kerf slots. The

wedges were cut off flush with the top of the handle, leaving the handle securely mounted hammer as shown in Figure 34.

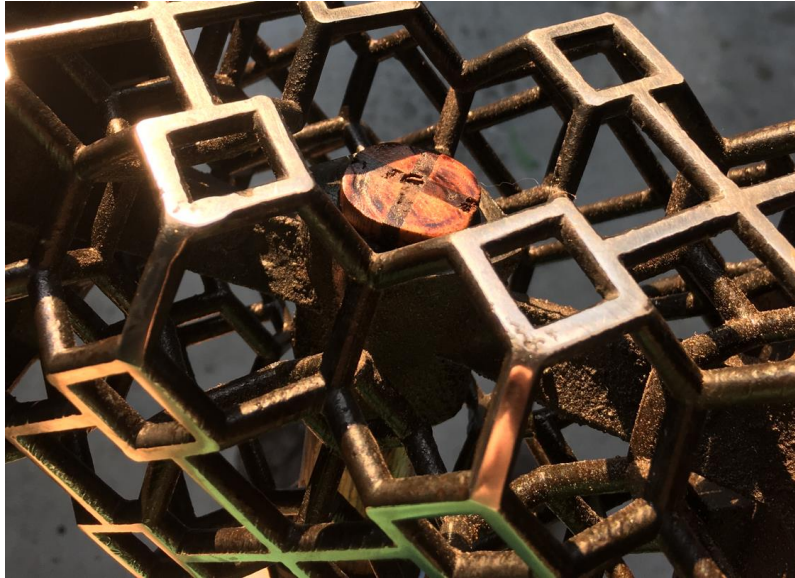


Figure 34: Handle Mounted Securely via Kerf-and-Wedge Process

4. Results and Discussion

4.1 Final Alloy Composition

Samples were collected prior to pouring at Carolina Metal Casting. These were used to obtain the exact chemistry composition of the obtained 8630 steel, shown in Table 4. For the 8630 Steel chemistry, the measured results are compared against ASTM A29 published standards. It was found that all alloying elements fell well within acceptable ranges published for 8630 steel. For this reason, it was deemed that the target chemistry was successfully achieved.

Table 4: Final 8630 Alloy Chemistry from Spectrometry Analysis

Alloy Element	Content (wt.%)	Target per ASTM A29 (wt %) [25]	Within Acceptable Range? (T/F)
Fe	97.1		
C	0.288	0.28-0.33	T
Si	0.332	0.15-0.35	T
Mn	0.788	0.70-0.90	T
P	0.0157	0.035 (max)	T
S	0.0062	0.040 (max)	T
Cr	0.522	0.40-0.60	T
Mo	0.198	0.15-0.25	T
Ni	0.632	0.40-0.70	T
Al	0.0315		
Cu	0.0765		
Ti	0.0022		
V	0.0039		

Unlike steel, cast irons are typically graded by mechanical properties rather than by alloy content. For this reason, chemistry ranges are not specified by ASTM standard and alloy content generally differs from foundry to foundry. The final achieved ductile iron chemistry is shown below in Table 5. Based on the Carbon and Silicon content, the carbon equivalent was calculated and found to be 4.17 according to Equation 3. This is below the eutectic composition, yielding a hypoeutectic ductile iron.

Table 5: Final Ductile Iron Alloy Chemistry from Spectrometry Analysis

Alloy Element	Content (wt.%)
Fe	93.7
C	3.36
Si	2.43
Mn	0.332
P	0.0221
S	0.0064
Cr	0.0275
Mo	0.0060
Ni	0.0113
Al	0.0094
Cu	0.0232
Mg	0.0400
Ti	0.0026
V	0.0022

Equation 3:
$$C.E. (wt\%) = C + \frac{1}{3}Si$$

4.2 Microstructure Analysis and the Bimetal Interface

From the bimetallic cast sample, it is clear that the proposed hypothesis was valid for the bimetal casting design. The experimental casting validates that Steel, poured at a temperature sufficiently above the solidus of iron, will form a robust fusion zone between the materials when poured onto solid iron. Figure 19 shown previously, depicting the bimetallic interface at a macro-scale, shows a seamless interface between the two materials. Figure 35 shown here provides higher magnification images of the interface between the two materials, demonstrating a unified metallurgical bond with no major defects.



Figure 35: Medium Magnification Image of Bimetal Interface As-Cast

The test sample was also heat treated in a similar manner as the actual hammer casting. The entire heat treatment procedure shown in Figure 32 was followed as closely as possible to predict the final microstructure of the hammer. A cross section of the sample was normalized twice and treated to convert the carbides to malleable iron. Following this stage, the sample was divided in half. Half of the sample was kept unquenched to examine the microstructure following the white iron treatment. The other half of the sample was then quenched to obtain the final microstructure present in the hammer. In this way, the as-cast, malleable iron treated, and quenched microstructures were all obtained for studying the final hammer microstructure.

After the malleable iron heat treatment, the sample was polished and examined unetched to show good contrast between the iron matrix and the graphite phase. From these images, it was found that finely dispersed malleable graphite nodules occurred evenly throughout the sample from the carbide dissolution as shown in the low magnification image in Figure 36. During the malleable iron treatment, carbon from the carbides will diffuse and nucleate, growing on nitrides and other precipitates in the iron matrix to near-nodular shape in order to minimize the total free energy of the system. A higher magnification image of the malleable graphite morphology is shown in Figure 37.

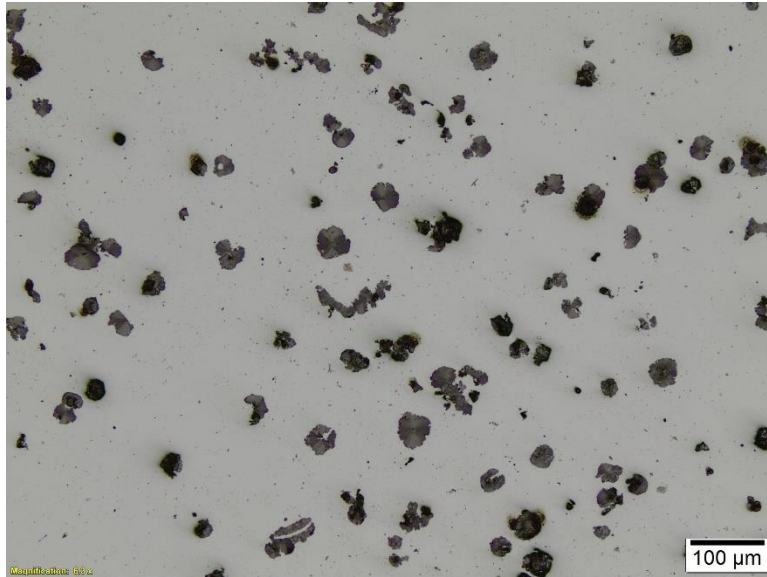


Figure 36: Low Magnification Image of the Malleable Iron Graphite Morphology

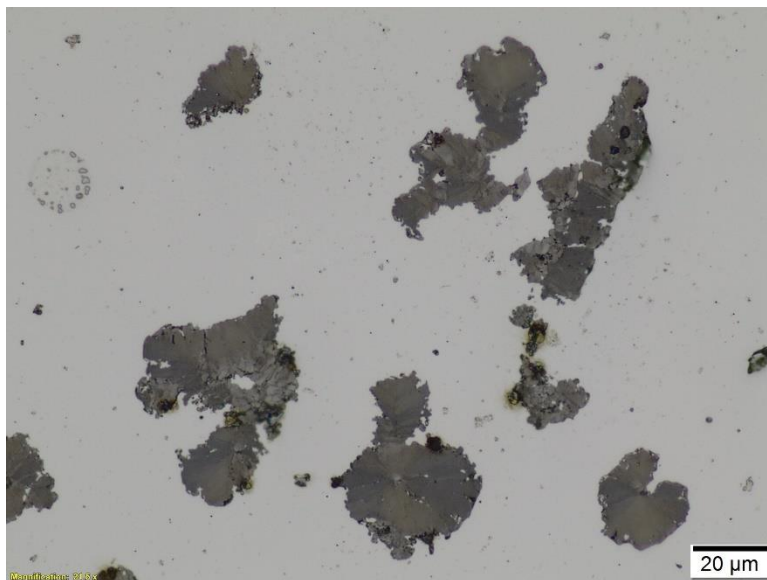


Figure 37: High Magnification Image of the Malleable Iron Graphite Morphology

After the malleable treatment, both the iron and the steel microstructures contain pearlite and ferrite. The samples were etched using a 2% Nital solution to expose the iron matrix. Figure X shows the etched medium magnification images of the cast iron matrix (Figure 38(a)) and the cast steel matrix (Figure 38(b)). As shown in Figure Xa, the coarse pearlite grain structure with significant amounts of ferrite indicates a slow cooling rate and low overall mechanical properties. The microstructure of steel shown in Figure 38(b) also contains significant ferrite content, resulting in low hardness.

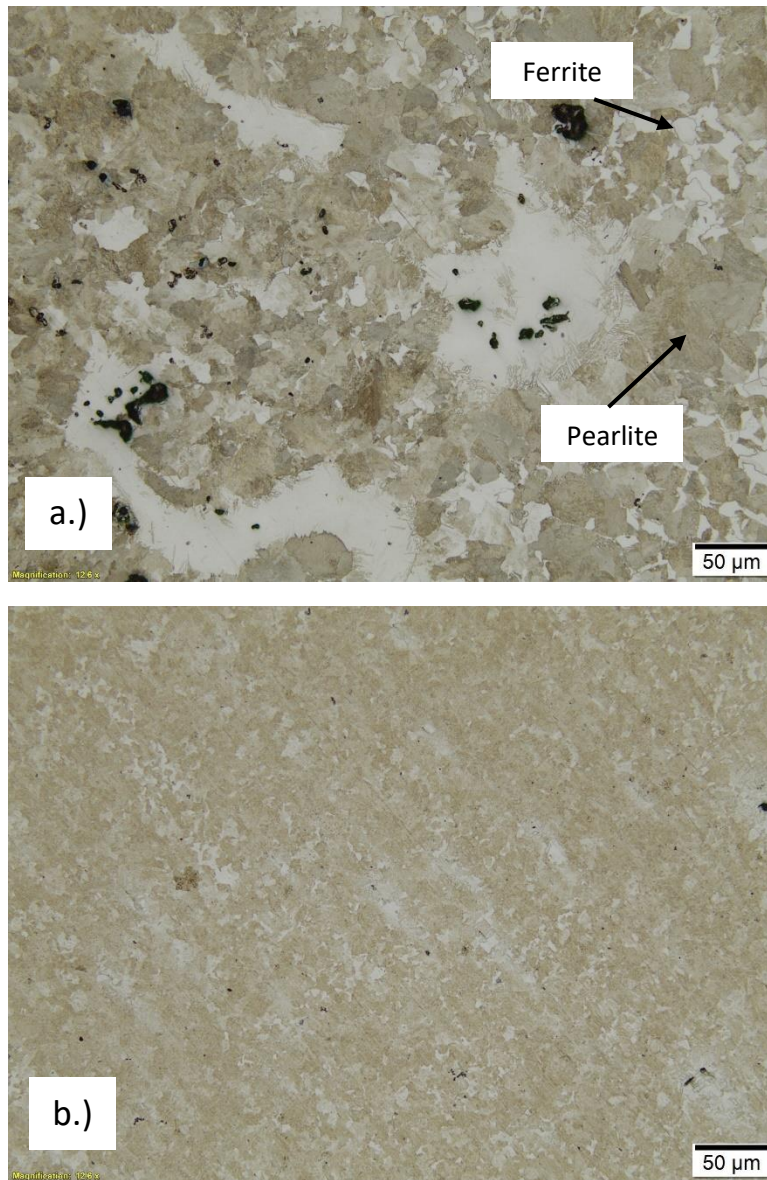


Figure 38: Medium Magnification Images of Unquenched Malleable Treated Cast Iron (a.) and Steel (b.)

After the sample was reaustenitized and quenched, the overall microstructure is very different and much better suited to impact tooling applications. The quench sample was deep etched to contrast the bainitic and martensitic grain structures. Figure 39 shows a clear contrast in the quenched cast iron microstructure of bainite mixed with martensite and malleable graphite. In the quenched cast iron sample, it is clearly shown why the ductile iron lattice should be well insulated against the quench effects. The blue acicular grains are upper bainite. Coarse acicular bainite grains are common sources of crack propagation and should be avoided.[23] Additionally, the grains which etched brown are plate martensite, which form at high carbon content and are mixed with retained austenite, which are observed in the white particles. Plate martensite is also quite brittle and known for crack propagation.

For this reason, it is more beneficial for the ductile iron lattice to resemble the unquenched microstructure than the quenched microstructure. Rockwell hardness readings of the quenched cast iron microstructure were taken and averaged at 59 RHC, far too hard and brittle for impact applications.

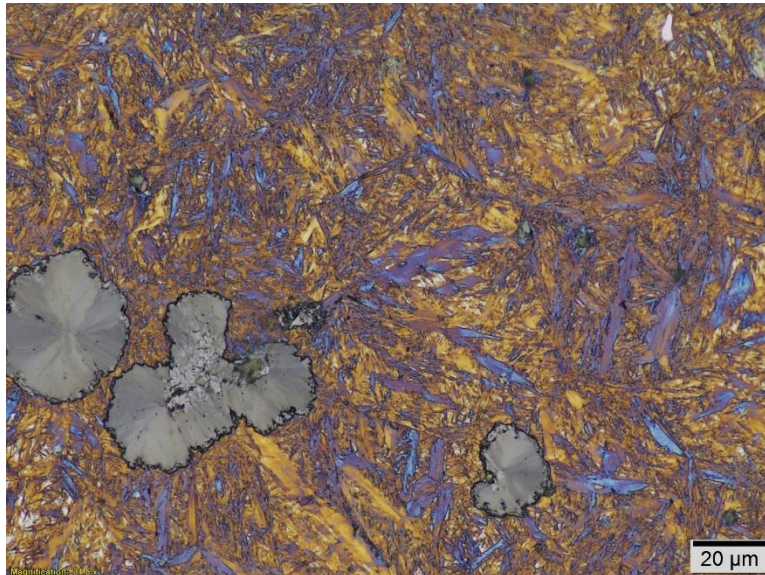


Figure 39: High Magnification Image of Quenched Cast Iron Matrix

Examining the quenched steel microstructure, a very fine microstructure of bainite and martensite is observed which is well suited to a combination of hardness and toughness. In Figure 40, a very fine matrix of evenly mixed bainite and lath martensite is observed. Unlike plate martensite, lath martensite is formed at lower carbon content. Of the martensite which forms, when the carbon content is under 0.5 wt% almost 80% of the martensite formed will be lath. [23] Because lath martensite is much finer and less acicular, after tempering, it will yield much higher toughness compared to plate martensite and is desired for medium hardness/high toughness applications. In Figure 40, the martensite appears as light tan-colored grains. The darker grains are bainitic. Bainite formation during quench is almost unavoidable as shown in the CCT curve for 8630 steel shown in Figure 23. Bainite shows a desirable combination of strength and ductility when it is not of coarse acicular morphology and in this case is highly desirable. The hardness of the quenched steel sample was found to be 45 RHC, almost exactly the target hardness for a quality hammer. This mixture of hardness and toughness was obtained through a mixed martensitic and bainitic microstructure obtained through quenching.



Figure 40: High Magnification Image of Quenched 8630 Steel Microstructure

4.3 Analysis of Fusion Defects in the Hammer Casting

As the sample weld experiment previously discussed showed excellent fusion at the interface, the most important question to discuss is why the lattice structure did not weld with the steel casting. Further experimentation will need to be done before a definitive answer can be given, but it is suspected that this could be attributed to differences in thermal expansion between the two materials. Because the thermal expansion of steel and iron differ, they will expand and contract at different rates, causing warping and uneven contraction during cooling which could have pulled the two interfaces apart.

Although the bimetal fusion between the two castings was not completely successful during the first production run, experimental validation shows that this indeed is a viable casting technique for a wide range of applications. By preheating the sand core prior to pouring, or by transitioning to investment casting techniques, it could be possible to ensure a complete metallurgical bond between the two castings, successfully harnessing the desirable material properties of both materials to address a single engineering application.

5. Conclusion

By further developing cutting edge research being performed in the field of metal casting and bimetal composites, the Georgia Southern Cast in Steel competition team successfully produced a bimetal Thor's hammer inspired by influences from Nordic mythology and the Marvel™ comic book universe. The hammer consisted of a hammer skeletonized structure cast in 8630 steel supported by a cast ductile iron lightweight lattice structure. This bimetal casting combined technology in additive manufacturing, investment casting, sand casting, heat treatment, and metallurgy to develop a unique engineering solution to the requirements put forward by the Steel Founder's Society of America. The

final casting weighed 5.3 lbs, featured an 18 inch goatskin wrapped hickory handle, and is capable of meeting the strenuous standards required for practical testing. By producing a hammer worthy of Thor, the Georgia Southern 2021 Cast in Steel competition team not only developed a casting capable of excelling in practical competition, but further developed what is achievable through bimetal composite casting.

Acknowledgements

The Georgia Southern University 2021 Cast in Steel team would like to thank several key individuals and groups which were instrumental in making this project a success. First and foremost, we would like to thank Dr. Mingzhi Xu and Dr. Jingjing Qing for their tireless efforts to encourage and support the team throughout the entire process. This project would not have been possible without their support, encouragement, and much needed advice. Next, we would like to offer a sincere thanks to Carolina Metal Casting in Hardeeville South Carolina for their roll in making this project happen. The attention and support the entire company provided to making this casting a success were absolutely invaluable and we cannot thank them enough. We would also like to thank Mr. Jeff Hoopes at Georgia Southern University for his advice and assistance in post processing and machining. As a team formed and operating through the Georgia Southern student chapter of the American Foundry Society, we would like to thank the many individuals who have made this organization a reality at our campus. Last, but certainly not least, we would like to offer a warm thanks to the Georgia Southern Department of Mechanical Engineering, and the Department of Manufacturing Engineering for their roles in supporting our team through facilities, equipment, and resources.

References:

- [1] McCoy, D., "Thor's Hammer," Norse Myth. Smart People [Online]. Available: <https://norse-mythology.org/symbols/thors-hammer/>.
- [2] Eliade, M., and Trask, W. R., 1959, *The Sacred and the Profane : The Nature of Religion.*, Harcourt, Brace & World.
- [3] "Club Hammers" [Online]. Available: <https://www.fullertool.com/product/club-hammers/>.
- [4] Thomas, R., and Buscema, J., 1966, "Thor (Marvel Comics)."
- [5] Farquhar, P., 2017, "Chris Hemsworth's Thor Hammer Could Be Yours for \$50,000," *Bus. Insid. Aust.*
- [6] El-Aziz, K. A., and Saber, D., 2020, "Mechanical and Microstructure Characteristics of Heat-Treated of High-Cr WI and AISI4140 Steel Bimetal Beams," *J. Mater. Res. Technol.*, **9**(4), pp. 7926–7936.
- [7] Wróbel, T., 2014, "Characterization of Bimetallic Castings with an Austenitic Working Surface Layer and an Unalloyed Cast Steel Base," *J. Mater. Eng. Perform.*, **23**(5), pp. 1711–1717.
- [8] Wróbel, T., 2011, "Ni AND Cr BASE LAYERS IN BIMETALLIC CASTINGS," *Mater. 20th Anniv. Int. Conf. Metall. Mater. – Met. 2011.*, pp. 758–764.
- [9] Zic, S., Dzambas, I., and Ikonc, M., 2009, "Possibilities of Implimenting Bimetallic Hammer Castings in Crushing Industries," **48**(1), pp. 51–54.
- [10] Zhong, T., He, K., Li, H., and Yang, L., 2019, "Mechanical Properties of Lightweight 316L Stainless Steel Lattice Structures Fabricated by Selective Laser Melting," *Mater. Des.*, **181**, p. 108076.
- [11] Williams, C. B., Cochran, J. K., and Rosen, D. W., 2011, "Additive Manufacturing of Metallic Cellular Materials via Three-Dimensional Printing," *Int. J. Adv. Manuf. Technol.*, **53**(1–4), pp. 231–239.
- [12] Chu, C., Graf, G., and Rosen, D. W., 2008, "Design for Additive Manufacturing of Cellular Structures," *Comput. Aided. Des. Appl.*, **5**(5), pp. 686–696.
- [13] Miyoshi, E., Takaki, T., Ohno, M., Shibuta, Y., Sakane, S., Shimokawabe, T., and Aoki, T., 2018, "Correlation between Three-Dimensional and Cross-Sectional Characteristics of Ideal Grain Growth: Large-Scale Phase-Field Simulation Study," *J. Mater. Sci.*, **53**(21), pp. 15165–15180.
- [14] 2018, *Steel Selection for Hardening.*
- [15] Górný, M., 2012, "Fluidity and Temperature Profile of Ductile Iron in Thin Sections," *J. Iron Steel Res. Int.*, **19**(8), pp. 52–59.
- [16] Dossett, J., and Totten, G. E., 2018, "Heat Treating of Low-Alloy Steels," *Heat Treat. Irons Steels*, **4**, pp. 122–168.
- [17] "From Ball-Peen to Top Set," *Blacksm. Organ. Arkansas.*
- [18] Horton, R. A., and Metalsmiths, P., 2018, "Investment Casting[1]," *Casting*, pp. 646–661.
- [19] Six, E., "Design of Gating and Feeding Systems," pp. 1–12.

- [20] Hayrynen, R. K., and Process, A., 2018, "Heat Treating and Properties of Ductile Iron," Heat Treat. Irons Steels, **15**(c), pp. 508–521.
- [21] Stefanescu, D. M., 2018, "Classification and Basic Metallurgy of Cast Iron[1]," Prop. Sel. Irons, Steels, High-Performance Alloy., **1**, pp. 3–11.
- [22] Ductility, T. H. E., 2018, "Heat Treatment of Malleable and Compacted-Graphite Irons," Heat Treat. Irons Steels, **4**(Ref 1), pp. 522–526.
- [23] Bhadeshia, H. K. D. ., and Honeycombe, R. W. ., 2017, *Steels: Microstructure and Properties*, Elsevier, Cambridge.
- [24] Athavale, V. A., 2019, "Scholars ' Mine Development of Stage-I Tempered High Strength Cast Steel for Ground Engaging Tools."
- [25] 2012, *ASTM A29*.